

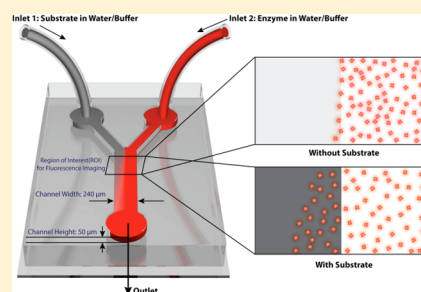
## Enzyme Molecules as Nanomotors

Samudra Sengupta,<sup>†</sup> Krishna K. Dey,<sup>†,§</sup> Hari S. Muddana,<sup>‡,§</sup> Tristan Tabouillot,<sup>†,‡,§</sup> Michael E. Ibele,<sup>†</sup> Peter J. Butler,<sup>\*,‡</sup> and Ayusman Sen<sup>\*,†</sup>

<sup>†</sup>Department of Chemistry, <sup>‡</sup>Department of Bioengineering, The Pennsylvania State University, University Park, Pennsylvania 16802, United States

### S Supporting Information

**ABSTRACT:** Using fluorescence correlation spectroscopy, we show that the diffusive movements of catalase enzyme molecules increase in the presence of the substrate, hydrogen peroxide, in a concentration-dependent manner. Employing a microfluidic device to generate a substrate concentration gradient, we show that both catalase and urease enzyme molecules spread toward areas of higher substrate concentration, a form of chemotaxis at the molecular scale. Using glucose oxidase and glucose to generate a hydrogen peroxide gradient, we induce the migration of catalase toward glucose oxidase, thereby showing that chemically interconnected enzymes can be drawn together.



## ■ INTRODUCTION

Enzyme-based biological motors perform specific cellular functions, such as DNA synthesis and vesicular transport, with great precision and efficiency.<sup>1–3</sup> On a higher level, biological motors also facilitate the directed movement (taxis) of cells toward specific chemicals or light.<sup>4,5</sup> In all cases, the movement arises from harnessing chemical free energy released through enzymatic turnover of substrates. A fundamental question that arises is whether a single enzyme molecule can generate sufficient mechanical force through substrate turnover to cause its own movement and, more significantly, whether the movement can become directional through the imposition of a gradient in substrate concentration, a situation that parallels the chemotaxis of whole cells. Positive answers to these questions have important implications in areas ranging from biological transport to the design of “intelligent,” enzyme-powered, autonomous nano- and micromotors, which are expected to find applications in bottom-up assembly of structures, pattern formation, cargo delivery at specific locations, roving sensors, and related functions.<sup>6–8</sup>

While it has been demonstrated that motion at the nano/microscale can be accomplished through catalysis-induced conversion of chemical energy to mechanical forces,<sup>7–15</sup> the use of enzymes as chemomechanical transducers would vastly expand the available methods for powering nano- and micromotors because of enzymes’ great diversity and efficiency. We have previously shown that the diffusion coefficient of urease molecules increases in the presence of its substrate, urea, in a concentration-dependent manner.<sup>16</sup> Here, we show that (a) the diffusive movement of catalase molecules also increases with increasing substrate concentration and (b) in the presence of a substrate concentration gradient, both enzymes diffuse toward areas of higher substrate concentration. Further, by employing a two-enzyme cascade, we show that chemically interconnected enzymes can be drawn together.<sup>17</sup>

## ■ RESULTS AND DISCUSSION

The diffusion coefficient of fluorescent-labeled catalase enzyme molecules was measured in solutions with varying hydrogen peroxide concentration, ranging from 1 mM to 100 mM, using fluorescence correlation spectroscopy (FCS). FCS is an ultrasensitive technique that can detect the motion of individual fluorescent molecules diffusing into and out of a diffraction-limited observation volume (1 to 2 fL).<sup>18</sup> A time-correlated single-photon counter (TCSPC) is incorporated in the instrument to measure the fluctuations in fluorescence intensity within the observation volume, arising from diffusion of the analyte molecules across the observation volume boundary.<sup>18</sup> The fluctuating fluorescence signal can then be autocorrelated and fitted to a theoretical three-dimensional (3-D) diffusion model to determine the analyte diffusion coefficient.<sup>19</sup> In our experiments, the presence of non-negligible amounts of free dye in the samples resulted in signatures of two diffusing components in the autocorrelation curves, and the curves were fitted to a two-component 3-D diffusion model: the fast component corresponding to the freely diffusing dye molecules, and the slow component corresponding to the fluorescent-labeled catalase molecules. The presence of hydrogen peroxide in the solution caused a significant increase in the diffusion of catalase molecules. The measured diffusion coefficient of catalase increased from  $6.0 \times 10^{-7}$  cm<sup>2</sup>/s in water to  $8.7 \times 10^{-7}$  cm<sup>2</sup>/s in 0.1 M hydrogen peroxide solution, an increase of 45% (Figure 1A). Moreover, the diffusion coefficient of the enzyme increased in a substrate-concentration-dependent manner.

To demonstrate that the enhanced enzyme diffusion was caused by substrate turnover, the diffusion coefficient of catalase inhibited by sodium cyanide<sup>20</sup> was measured in the

Received: September 20, 2012

Published: January 10, 2013

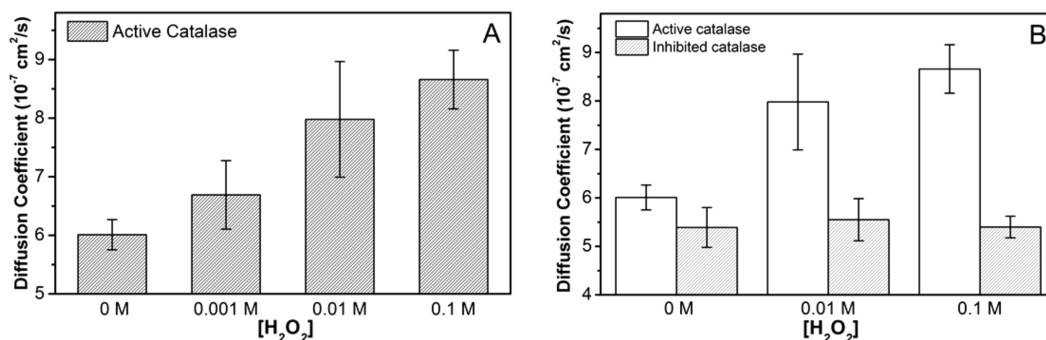


**Figure 1.** Diffusion studies of catalase enzyme. (A) Diffusion coefficient of catalase enzyme increased up to  $\sim 45\%$  with increasing concentration of its substrate, hydrogen peroxide. Diffusion coefficients of catalase at different hydrogen peroxide concentrations (0.001, 0.01, 0.1 M) are significantly different from that of water (0 M) (significance value of  $P < 0.01$ ). (B) Increase in catalase diffusion coefficient was significantly attenuated in the presence of catalase inhibitor, sodium cyanide. Diffusion coefficients of inhibited catalase at different hydrogen peroxide concentrations (0.01 and 0.1 M) are not significantly different from that of water (0 M) (significance value of  $P > 0.01$ ). Error bars represent standard deviations. The means and standard deviations are calculated for 10 different independent measurements.

presence of substrate, and no significant change in diffusion was observed (Figure 1B). As with urease,<sup>16</sup> the force exerted on this enzyme due to substrate turnover was estimated to be  $\sim 10$  pN/turnover using Brownian dynamics simulations. This value is well within the range of the forces measured for other molecular-scale systems, including polymerases and motor proteins.<sup>21–23</sup>

Enhanced diffusive motion at the single-molecule level in the presence of a substrate led us to hypothesize that enzyme molecules might exhibit collective directional diffusion in the presence of a substrate gradient.<sup>24,25</sup> Accordingly, a fluorescence imaging setup was used to characterize enzyme movement along a substrate concentration gradient. A Y-shaped microfluidic channel with two inlets—one for fluorescently-labeled enzyme in water/buffer and the other for just water/buffer or substrate in water/buffer—was used to generate the substrate gradient (Figure 2). The flow rate

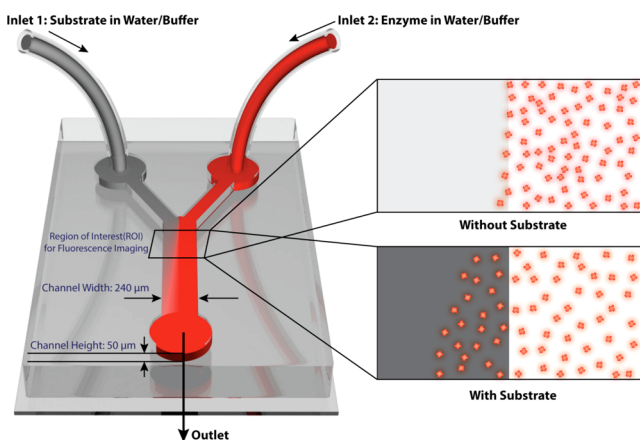


**Figure 2.** Schematic representation of the Y-shaped microfluidic channel used for chemotactic studies of ensembles of enzyme molecules.

through each of the two inlets was held constant at  $15 \mu\text{L}/\text{h}$ , which corresponds to an average linear (laminar) flow of  $694 \mu\text{m}/\text{s}$  in the main channel. This value of average laminar flow is obtained from the volumetric flow rate of the fluid and cross-sectional area of the microchannel. Lateral spreading of the enzyme at a defined location in the microchannel was fluorescently measured in the presence and absence of the

substrate. The fluorescence intensity plots were normalized (1 corresponds to maximum intensity, and 0 corresponds to minimum intensity) to calculate the shift at a fixed value of fluorescence intensity. The directional behavior was studied for both catalase and urease enzymes with their corresponding substrates, hydrogen peroxide and urea. A shift in normalized fluorescence intensity across the channel was observed for catalase toward the region of the channel containing its substrate, 10 mM hydrogen peroxide, as compared to no substrate (Figure 3A). The lateral shift in normalized fluorescence intensity in the region of interest (ROI) ( $\sim 400 \mu\text{m}$  down the channel) was  $13.3 \mu\text{m}$ . This shift was highly attenuated when the enzyme was inhibited (Figure 3A). The fluorescence intensity profile of this inhibited catalase exposed to a flow containing 10 mM hydrogen peroxide was comparable to that of active catalase exposed to a flow containing no substrate, indicating that catalytic substrate turnover was responsible for the movement of enzyme molecules toward higher substrate concentrations.

Similar to catalase, urease enzyme molecules spread toward the region of the channel containing urea (Figure 3B). A lateral shift in normalized fluorescence intensity of  $9.2$  and  $11.5 \mu\text{m}$  was observed in the presence of 1 M urea, as compared to no substrate, as measured in the ROI,  $\sim 400 \mu\text{m}$  (Figure 3B) and  $\sim 900 \mu\text{m}$  (see Figure S1, Supporting Information [SI]) down the channel, respectively. The non-normalized plots reflect the expected broadening of the fluorescence intensity profile for urease in the presence of urea, as compared to buffer (see Figure S2, SI).

In order to rule out the effect of lateral flow and convection, identical experiments were performed with free rhodamine and Dylight 549 dye molecules (the same dyes used to label the enzymes) in the presence of hydrogen peroxide or urea gradients. No lateral shifts were observed for rhodamine dye in the presence of hydrogen peroxide gradients (Figure 4A). In the case of Dylight 549 dye a slight shift *away* from the urea gradient was observed (see Figure S3A, SI).

It is possible that formation of oxygen during decomposition of hydrogen peroxide by catalase, and hydrolysis of urea by urease can cause distortion of the flow profiles and bulk lateral movement of fluid, which may result in the observed collective spreading behavior. To rule out such an effect, we introduced 20 nm quantum dots (QDots) in the inlet with catalase (unlabeled), and studied their lateral spreading in the presence

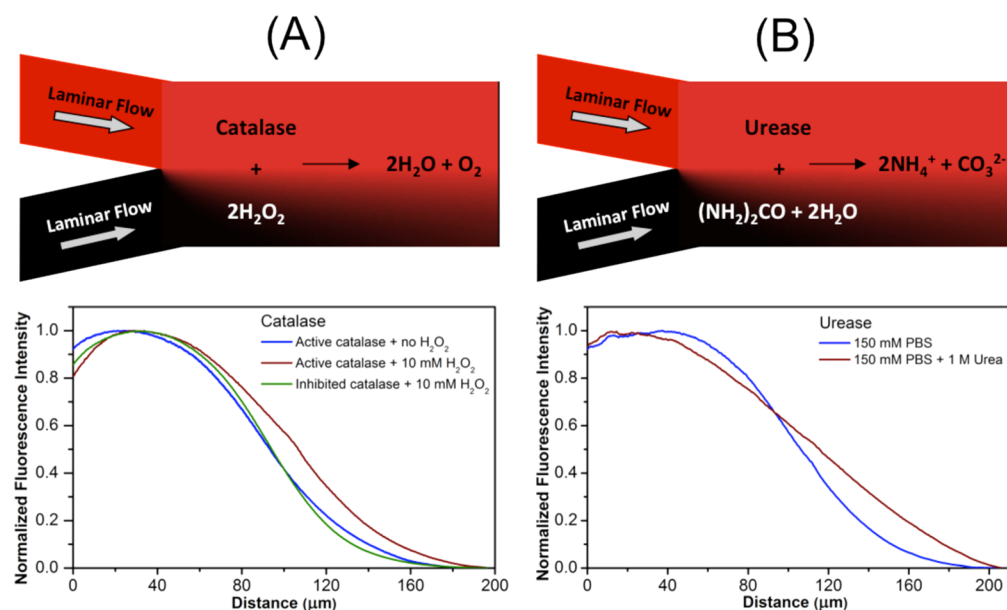


**Figure 3.** Chemotaxis of catalase and urease enzyme molecules. (A) Plot of mean normalized fluorescence intensity (arbitrary units; ‘1’ corresponds to maximum fluorescence intensity and ‘0’ corresponds to minimum fluorescence intensity) profile as a function of lateral position along the width of the channel showed a shift for catalase toward 10 mM hydrogen peroxide (red; *maximum standard deviation of 0.039 au*), as compared to water (blue; *maximum standard deviation of 0.003 au*), when evaluated at  $\sim 400 \mu\text{m}$  from the channel inlet. The shift in fluorescence intensity profile of the inhibited catalase (green; *maximum standard deviation of 0.121 au*) in the presence of 10 mM hydrogen peroxide was comparable to that of active catalase in water. (B) Plot of mean normalized fluorescence intensity profile as a function of lateral position along the width of the channel showed a shift for urease toward 1 M urea in 150 mM PBS buffer (red; *maximum standard deviation of 0.012 au*), as compared to 150 mM PBS buffer (blue; *maximum standard deviation of 0.037 au*), when viewed  $\sim 400 \mu\text{m}$  from the start of the channel.

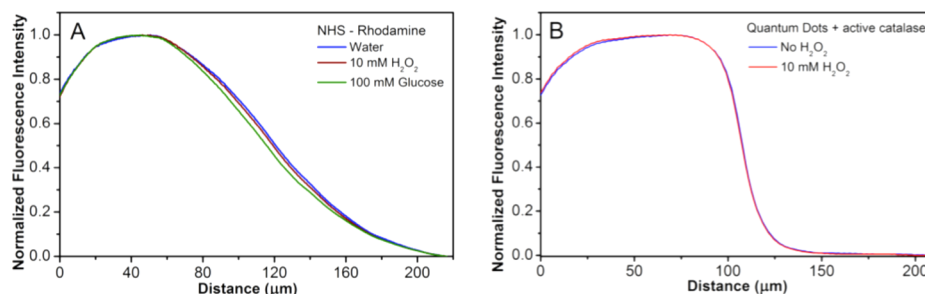


**Figure 4.** Behavior of free dye molecules and quantum dots (QDots) toward substrate concentration gradients. (A) Plot of mean normalized fluorescence intensity profile as a function of position along the width of the channel. This plot indicates that there is no shift for NHS-Rhodamine dye (used to label catalase) toward 10 mM hydrogen peroxide (red) or 100 mM glucose (green), compared to water (blue). (B) Lateral spreading of 20 nm QDots flowed through the inlet with active catalase (unlabeled) in the presence and absence of a gradient of hydrogen peroxide (flowed through the other inlet) showed no shift in fluorescence intensity toward 10 mM hydrogen peroxide (red) as compared to water (blue).

and absence of a gradient of hydrogen peroxide (flowed through the other inlet). No shift in fluorescence intensity was observed for QDots in the presence of active catalase toward 10 mM hydrogen peroxide as compared to water (Figure 4B). Similar observations with urease showed a slight shift in fluorescence intensity for QDots away from 1 M urea as compared to buffer (see Figure S3B, SI). The above results indicate that the collective spreading behavior observed for both catalase and urease toward their respective substrates do not arise from enzymatic reaction-induced distortion of bulk fluid flows.

The fluorescence intensity profiles were measured at a depth, which is the centerline of the microfluidic channel, to rule out the effect of the channel walls on the flow profile. To further exclude the effect of the channel walls (lower glass surface and upper polydimethylsiloxane surface), collective migration experiments with urease enzyme were performed using a

confocal microscope. The plane of imaging was carefully chosen such that the fluorescence intensity profiles were recorded at halfway depth inside the microfluidic device. Using a 2-inlet microfluidic device, urea was flowed through one of the inlets to generate a substrate concentration gradient. The fluorescently-tagged enzyme was flowed through the other inlet. A laminar flow rate of  $1.85 \times 10^4 \mu\text{m/s}$  was maintained through the main channel, and lateral spreading of urease enzyme molecules at  $\sim 4000 \mu\text{m}$  down the channel was fluorescently measured in the presence and absence of a urea concentration gradient. A shift in normalized fluorescence intensity of  $4.5 \mu\text{m}$  (in the ROI) was observed in the presence of urea as compared to buffer (Figure 5).

The above results suggest that an enzyme that acts on the products of a second, nearby enzymatic reaction might exhibit movement up the substrate gradient toward this second enzyme; an example of collective behavior at the molecular

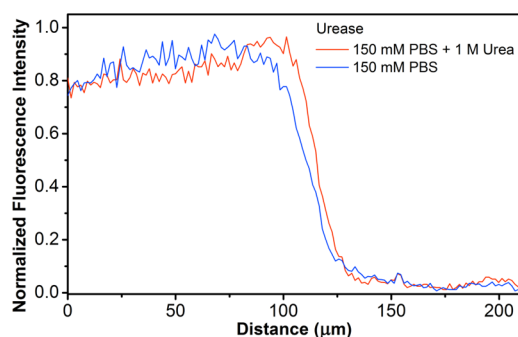


**Figure 5.** Plot of mean normalized fluorescence intensity profile as a function of lateral position along the width of the channel showed a shift for urease toward 1 M urea in 150 mM PBS buffer (red; maximum standard deviation of 0.1 au), as compared to 150 mM PBS buffer (blue; maximum standard deviation of 0.08 au), when viewed under a confocal microscope.

level. We tested this hypothesis by choosing another enzyme, glucose oxidase (GOx), that catalyzes the oxidation of glucose to D-glucono- $\delta$ -lactone and hydrogen peroxide. Hydrogen peroxide released from the oxidation of glucose, in turn, serves as the substrate for catalase. The chemotactic behavior of catalase in the presence of GOx and 100 mM glucose was studied by introducing catalase through one inlet of the microfluidic channel, and GOx and glucose through the other. A large lateral shift in the normalized fluorescence intensity profile of catalase across the channel was noted when both GOx and glucose were introduced through the second inlet, as compared to only glucose (Figure 6 and see Figure S4, SI). The lateral shift corresponds to 21.4  $\mu\text{m}$  as analyzed in the ROI ( $\sim 400 \mu\text{m}$  down the channel). The non-normalized plot reflects the expected broadening of the fluorescence intensity profile for catalase in the presence of GOx and glucose, as

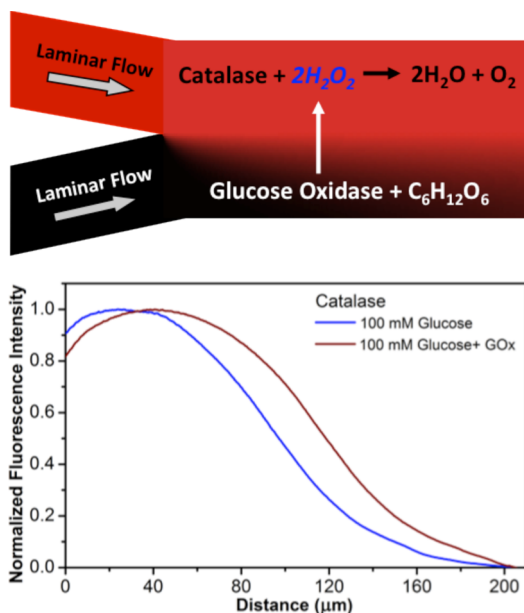


**Figure 6.** Plot of mean normalized fluorescence intensity profile as a function of lateral position along the width of the channel indicated a shift of catalase toward 100 mM glucose and glucose oxidase (red; maximum standard deviation of 0.033 au), as compared to 100 mM glucose (blue; maximum standard deviation of 0.018 au), when viewed  $\sim 400 \mu\text{m}$  from the start of the channel.

compared to glucose only (see Figure S5, SI). The relatively large lateral shift was due to essentially complete conversion of glucose within the time frame of the experiment. The experiment clearly demonstrates that catalysis-induced directional movement of enzymes can lead to collective attraction between two different enzymes.

The experimentally observed chemotaxis by enzyme ensembles was simulated using COMSOL Multiphysics (v4.3)—by coupling the physics of laminar flow and transport of dilute species in a fluid. The simulation geometry was defined in 2-D as a microchannel of length 3 mm and width of 240  $\mu\text{m}$ —with two inlets and a single outlet, similar to the microchannel geometry used in the experimental setup. The lower inlet allowed the flow of enzymes in water/buffer at a constant speed of 694  $\mu\text{m s}^{-1}$ . Through the upper inlet, first the solution of only water/buffer was introduced at the same flow speed, and the simulation was run to get the steady-state concentration profile of the enzymes across the channel, which arises mainly due to the transverse diffusive mixing of two parallel flows. The simulation was then repeated with the flow of substrate solution through the upper inlet and setting the diffusion coefficient of the enzyme as a function of local substrate concentration. The functional dependence of enzyme diffusion coefficient on substrate concentration was determined by fitting the experimentally recorded data (see Figures S6 and S7, SI). The simulation in this case yielded a concentration profile of enzymes in the presence of a substrate gradient. Relative magnitudes of the concentration profiles in the absence and presence of substrates in the upper inlet showed the enhanced migration of these enzymes up toward the upper inlet in the presence of a substrate. The simulated enhanced migrations of the enzyme ensemble, in both the cases of urease ( $\sim 2 \mu\text{m}$ ) and catalase ( $\sim 6 \mu\text{m}$ ) in the presence of their respective substrates, are within the same order of magnitude as obtained in the experimental results (Figure 7). In Figure 7, normal diffusion corresponds to the random diffusion of enzyme molecules in the absence of any substrate, whereas the collective directional migration of the enzyme molecules in the presence of a gradient in the substrate concentration has been referred to as enhanced diffusion. The simulation results suggest that *only* a substrate-dependent increase in diffusivity of enzyme molecules is sufficient for their collective migration toward higher substrate concentrations.

While the exact mechanism for the observed substrate-induced enhanced diffusion of the enzymes remains unclear, several possible alternative causes can be ruled out. The presence of the substrate and the products derived therefrom had a negligible effect on solvent viscosity (see Figure S8, SI). Addition of hydrogen peroxide up to 0.1 M did not result in a significant change in solution pH. The estimated rise in the bulk solution temperature due to enzymatic decomposition of hydrogen peroxide was too small to explain the observed increase in the diffusion coefficient (see SI). However, the possibility that enhanced diffusion arises from an instantaneous rise in temperature in the immediate vicinity of the enzyme molecule cannot be ruled out.

The decomposition of hydrogen peroxide by catalase results in the formation of water and oxygen, and at higher concentrations of peroxide, gas bubbles form in solution. Although care was taken not to take data from regions of the fluid perturbed by visible bubbles, self-propulsion of microscale catalytic motors due to visible bubble generation has been reported in the past.<sup>26,27</sup> To test the effect of bubble formation

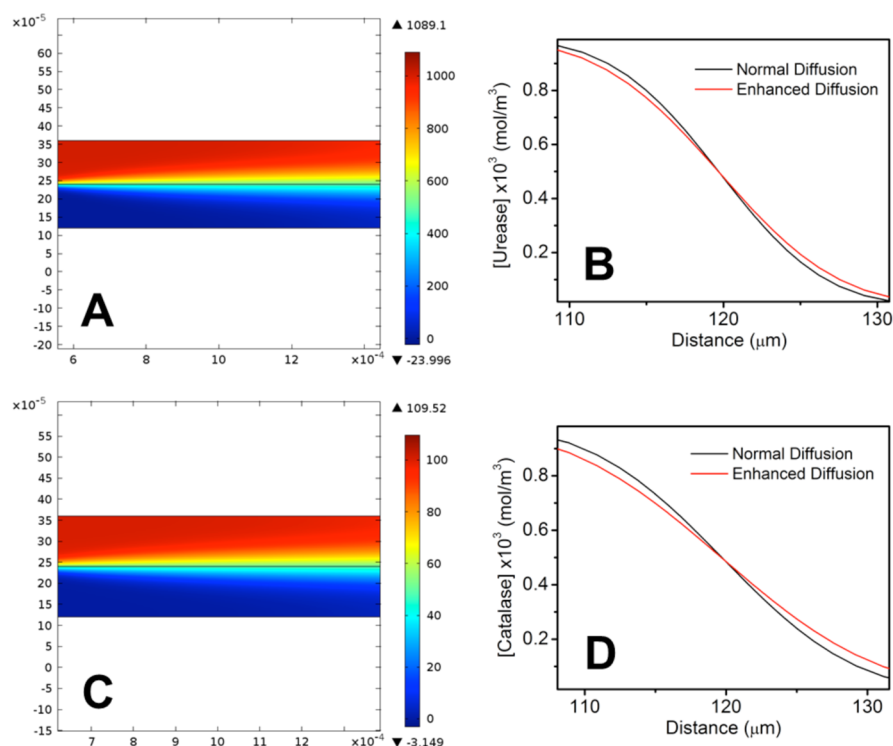


**Figure 7.** (A) Simulated steady state concentration gradient of urea established along the interface (maximum and minimum concentrations are indicated in red and blue, respectively). (B) Simulated steady state concentration profile of urease across the microchannel interface, showing the enhanced migration of enzymes toward higher substrate concentrations. (C) Simulation results showing steady state concentration gradient of hydrogen peroxide established along the interface (maximum and minimum concentrations are indicated in red and blue, respectively). (D) Simulation results showing steady state concentration profile of catalase across the microchannel interface, showing the enhanced migration of enzymes toward higher substrate concentrations.

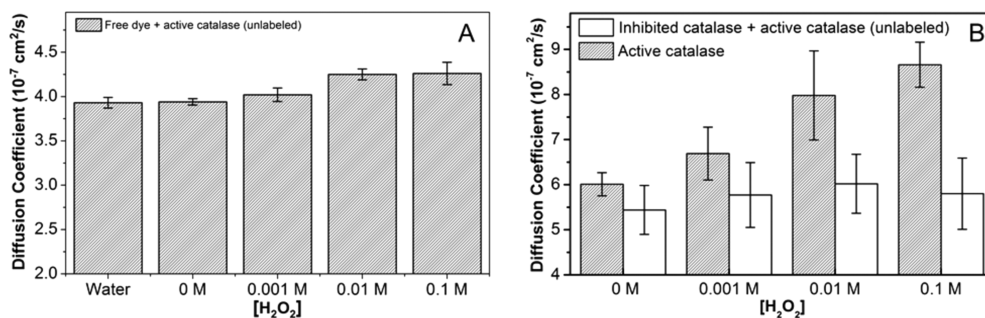


**Figure 8.** (A) Diffusion coefficient of free NHS-Rhodamine dye molecules in the presence of *unlabeled* active catalase and hydrogen peroxide showed only a slight increase of  $\sim 7\%$  at higher substrate concentrations. (B) Diffusion coefficients of fluorescently labeled inhibited catalase in the presence of unlabeled active catalase at different hydrogen peroxide concentrations (0.001, 0.01, 0.1 M) were not significantly different from that of water (0 M) (significance value of  $P > 0.01$ ). Error bars represent standard deviations. The means and standard deviations are calculated for 10 different independent measurements.

elsewhere in the system on the local molecular diffusion, we measured the diffusion coefficient of free-dye (NHS-Rhodamine) molecules in the presence of unlabeled active catalase and hydrogen peroxide. A slight increase of  $\sim 7\%$  in free-dye diffusion was observed at higher substrate concentrations (Figure 8A). To further ascertain whether bubble formation was playing a role in the observed enhancement in diffusion, the diffusion coefficient of fluorescent-labeled inhibited catalase in the presence of active unlabeled catalase and hydrogen peroxide was measured. The inhibited catalase did not show a significant increase in diffusion, despite the formation of bubbles in solution (Figure 8B). The active and inactive enzymes were mixed with different hydrogen peroxide solutions

immediately before the diffusion measurements were performed. To rule out the effect of any residual cyanide ion (from the inhibited catalase) on the active enzyme, an activity assay was performed. The decomposition of hydrogen peroxide, monitored using a UV-vis spectrophotometer, was assessed in the presence of active catalase, inactive catalase, and a mixture of active and inactive catalases (Figure 9). The hydrogen peroxide decomposition profile for inactive catalase was very similar to that with no enzyme. The decomposition profiles for active catalase and the mixture show a similar trend, thereby eliminating the possibility that residual cyanide from the inactive catalase was also inhibiting the active enzyme molecules. Together, these results confirm that bubble

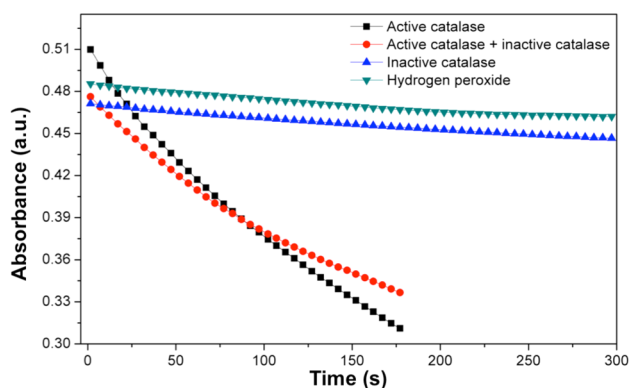


**Figure 9.** Decomposition of hydrogen peroxide was monitored using a UV–vis spectrophotometer in the presence of active catalase, inactive catalase, and a mixture of active and inactive catalases. The hydrogen peroxide decomposition profile for inactive catalase was very similar to that with no enzyme. The decomposition profiles for active catalase and a mixture of active and inactive enzyme showed a similar trend. The mean activity of the active enzyme sample was found to be 5791 units/mg of the solid (*standard deviation of 318 units/mg*). The sample of the mixture of active and inactive catalases showed a similar mean activity of 5390 units/mg of the solid (*standard deviation of 674 units/mg*). Mean and standard deviation are calculated for three measurements.

generation is not a viable mechanism for the observed enhanced diffusion at the single-molecule level. Also, gas molecules are not generated in the case of urease and, therefore, cannot be responsible for the observed enhancement in diffusion coefficient<sup>16</sup> and the directional movement of urease in response to urea gradient. It is possible, however, that the observed slight increase in diffusivity of the spectator-dye molecules results from other mechanisms such as hydrodynamic interactions<sup>28–30</sup> between the enzyme and free-dye molecules or local thermal heating.<sup>31</sup>

Movement arising from phoretic mechanisms such as diffusiophoresis, osmophoresis, and self-electrophoresis has been demonstrated in the past for catalytic particles.<sup>9,12</sup> In the current experiments, similar enhancements in diffusion were observed for catalase and urease,<sup>16</sup> even though the products formed in these reactions are neutral and ionic, respectively. Schwartz has also reported analogous observations for RNA polymerase.<sup>25</sup> This suggests that electrophoretic forces play, at best, a minor role in the observed enhanced diffusion.

The asymmetric placement of catalytic sites can lead to chemical gradients due to the asymmetric production of the reaction products (charged or uncharged). This, in turn, can drive the movement of catalyst particles.<sup>32–35</sup> However, such a mechanism is unlikely to apply to molecules that have symmetrically located catalytic sites. Moreover, even if these catalytic sites were undergoing reactions asynchronously, the concentration of the reaction products in the vicinity of the enzyme would be normalized almost instantaneously due to the fast rotational times of the relatively small enzyme molecule and the fast diffusion times of the reaction products, thus preventing the generation of a sustained chemical gradient. On the other hand, theoreticians have proposed that enzymes may “swim” due to nonreciprocal conformational changes that occur during substrate turnover.<sup>36–38</sup> Our observations may constitute experimental evidence for this hypothesis.

We hypothesize that the chemotactic behavior of the enzyme molecules arises from an enhanced diffusion mechanism.<sup>24,25</sup> The substrate gradient is analogous to a Brownian ratchet.<sup>39</sup> Many molecular machines in living systems function as Brownian ratchets.<sup>40,41</sup> In the present case, the substrate concentration changes continuously as the enzyme diffuses along the gradient. Thus, at every point in space, the diffusion rate increases on moving up the gradient and decreases on moving down the gradient. A higher diffusion coefficient leads to a greater spreading of the enzyme molecules on the side of the higher substrate concentration. As can be seen in the non-normalized plots (see Figures S2 and S5, SI), the “center of gravity” of the enzyme ensemble moves toward higher substrate concentration. As with any other Brownian ratchet, a continuous energy input is required for the directional movement, in this case to maintain the substrate gradient. The proposed mechanism is stochastic in nature and is different from biological chemotaxis, which requires temporal memory of the concentration gradient.

## CONCLUSION

We have explored the diffusive movement of catalase enzyme molecules in the presence of a concentration gradient of hydrogen peroxide, the substrate for the enzyme. The diffusion coefficient of catalase is enhanced in the presence of its substrate, increasing in a substrate concentration-dependent fashion. The increase in enzyme diffusivity can be attributed to substrate turnover, since the diffusivity of the inhibited enzyme did not increase in the presence of hydrogen peroxide. Controls with free dye and a mixture of active (unlabeled) and inactive (labeled) catalase in the presence of hydrogen peroxide show either a small or no change in diffusion, which rules out bubble-driven bulk convective flows as being responsible for increased enzyme diffusive motion.

We also showed that, in the presence of a substrate concentration gradient, ensembles of urease and catalase enzyme molecules show collective movement toward higher concentrations of urea and hydrogen peroxide, respectively. COMSOL Multiphysics simulations also showed a shift in the distribution of enzyme molecules toward higher substrate concentrations. In addition, we generated a concentration gradient of hydrogen peroxide by using glucose and glucose oxidase and showed collective migration of an ensemble of catalase molecules toward glucose oxidase. This is a form of predator–prey behavior at the molecular level. We hypothesize that the chemotactic behavior exhibited by the enzyme molecules arises from an enhanced diffusion mechanism.

One of the reviewers has suggested the possibility that the observed enhanced diffusion of enzymes may be due to bulk convective fluid flow due to the generation of oxygen bubbles or other extraneous factors related to enzymatic catalysis. Although this possibility cannot be completely ruled out, it is inconsistent with the results of our experiments with inactive catalase (labeled) and active catalase (unlabeled) in the presence of hydrogen peroxide (Figure 8B). The inhibited catalase, which acts as a spectator, does not show any increase in diffusion, suggesting the absence of any bulk convective flows. This is further supported by Figure 8A, where the diffusion coefficient of smaller free-dye molecules showed only a slight increase in the presence of active catalase (unlabeled) and hydrogen peroxide. While we consider these experiments to be conclusive, some caution needs to be exercised while interpreting multicomponent FCS fits. Bulk flows also appear

not to be important in the experiments demonstrating collective migration of enzyme molecules in a substrate gradient. We base this conclusion on results shown in Figure 4B and Figure S3B (SI). Control experiments with QDots in the inlet with catalase (unlabeled) showed no lateral spreading (Figure 4B) in the presence of a gradient of hydrogen peroxide as compared to water (flowed through the other inlet). Similar observations with urease showed no significant lateral migration for Qdots (see Figure S3B, SI) in the presence of urea as compared to that in buffer.

Our findings may open up new avenues in the field of enzyme-based devices such as intelligent enzyme-powered drug delivery vehicles, self-assembly of biomolecules, separation of catalyst molecules based on activity, among others.

## ■ EXPERIMENTAL METHODS

**Fluorescent Labeling of Urease and Catalase.** Jack bean urease (type C-3; Sigma-Aldrich) (see Figure S9A, SI) was tagged with a thiol-reactive dye, Dylight 549 (ex/em: 549/568; Thermo Fisher Scientific). The reaction of the fluorescent probe (40  $\mu$ M) with urease (2  $\mu$ M) was carried out in 150 mM phosphate buffer (pH 7) at room temperature for 2–6 h under gentle stirring (see Figure S9C, SI). Bovine liver catalase (Sigma-Aldrich; see Figure S9B, SI) was labeled with an amine-reactive rhodamine dye (ex/em: 552/575; Thermo Fisher Scientific). Labeling of catalase (4  $\mu$ M) with the fluorescent dye (40  $\mu$ M) was performed in a gently stirred, room temperature, 100 mM phosphate buffer (pH 7.2) for 2–3 h (see Figure S9D, SI). The enzyme–dye complexes were further purified using membrane dialysis (10 kDa pores; Amicon ultra-4 centrifugal filter unit, Millipore) to reduce free-dye concentration. The number of dye molecules per catalase enzyme molecule was  $\sim 2$  as quantified using UV–vis spectroscopy.

**Catalase Inhibition Studies.** Inhibition studies were performed using 0.5 M NaCN as the inhibitor.<sup>20</sup> Fluorescently labeled catalase (4  $\mu$ M) was incubated with the inhibitor in deionized water overnight. Membrane dialysis (10 kDa pores; Amicon ultra-4 centrifugal filter unit, Millipore) was used to separate the enzyme–dye complex from unreacted inhibitor.

**Single-Molecule Spectroscopy and Data Analysis.** Spectroscopy measurements were performed on a custom-built microscope-based optical setup, described previously.<sup>18</sup> Briefly, excitation light from a PicoTRAIN 532 nm, 80 MHz, 5.4 ps pulsed laser (High-Q Laser) was guided through an IX-71 microscope (Olympus), with an Olympus 60 $\times$ /1.2-NA water-immersion objective. Emitted fluorescent light from the sample was passed through a dichroic beam splitter (Z520RDC-SP-POL, Chroma Technology) and focused onto a 50  $\mu$ m, 0.22-NA optical fiber (Thorlabs), which acted as a confocal pinhole. The signal from the photomultiplier tube was routed to a preamplifier (HFAC-26) and then to a time-correlated single-photon counting (TCSPC) board (SPC-630, Becker and Hickl). The sample was positioned with a high-resolution 3-D piezoelectric stage (NanoView, Mad City Laboratories).

Fluorescent molecules moving in and out of the diffraction-limited observation volume induce bursts in fluorescence collected in first-in, first-out mode by the TCSPC board, which was incorporated in the instrument. Fluctuations in fluorescence intensity from the diffusion of molecules were autocorrelated and fit by a multicomponent 3D model (eq 1, see Figure S10, SI) to determine the diffusion coefficients of individual species,<sup>19,42,43</sup>

$$G(\tau) = \sum_{i=1}^n \frac{1}{N_i} \left[ 1 + \left( \frac{\tau}{\tau_D^i} \right) \right]^{-1} \left[ 1 + \left( \frac{1}{w} \right)^2 \left( \frac{\tau}{\tau_D^i} \right) \right]^{-1/2}, \quad \tau_D^i = \frac{r^2}{4D_i} \quad (1)$$

where  $N_i$  is the average number of fluorophores of  $i$ th species in the observation volume,  $\tau$  is the autocorrelation time,  $w$  is the structure factor ( $\sim 4$ – $8$ ), and  $\tau_D^i$  is the characteristic diffusion time of the fluorophores of  $i$ th species with diffusion coefficient  $D_i$  crossing a

circular area with radius  $r$  ( $\sim 400$  nm). Fluorescence correlation spectroscopy (FCS) measurements were performed with 60  $\mu$ W excitation power, and the optical system was calibrated before each experiment using free Rhodamine 6G (R6G) dye ( $D = 2.8 \times 10^{-6}$  cm<sup>2</sup>/s in water,<sup>19</sup> Invitrogen) in deionized water. Autocorrelation curves were fit to eq 1 using Levenberg–Marquardt nonlinear least-squares regression algorithm with Origin software to determine  $\tau_D^i$ . In our experiments, the presence of non-negligible amounts of free dye in the samples resulted in signatures of two diffusing components in the autocorrelation curves, and the curves were fitted to a two-component 3-D diffusion model—the fast component corresponding to the freely diffusing dye molecules and the slow component corresponding to the fluorescent-labeled catalase molecules.

The average concentrations of enzyme molecules in all the FCS measurements were identical within  $\pm 1$  molecule in the observation volume. The structure factor,  $w$ , was determined prior to measuring the enzyme diffusion coefficient, using the known diffusion coefficient of R6G, and was fixed for all subsequent measurements. Moreover, the structure factor was calibrated prior to each experiment. The diffusion coefficient of the free dye (used to label enzyme molecules) was also measured independently using a pure dye sample in the presence of catalase (unlabeled) and different hydrogen peroxide concentrations (as used in our experiments) (Figure 8A), and fixed during the curve-fitting process (for the enzyme sample). Characteristic diffusion time of the enzyme and the enzyme-to-free dye fraction were the only adjustable parameters during the fitting process.

It is important to note that the characteristic diffusion time determined using fluorescence correlation spectroscopy (FCS) is independent of the molecular brightness of the molecule.<sup>44</sup> Only fluctuations in the intensity contribute to the autocorrelation trace. Fluctuations in molecular fluorescence intensity due to fast processes such as triplet state excitation occur on a time scale much smaller than the characteristic diffusion time of the molecule and therefore do not affect the measured diffusion time. Moreover, the triplet state contributions were not apparent in the autocorrelation curves and therefore were not included in the fitting equation.

**Statistical Significance Analysis.** Student's  $t$  test was performed to verify the statistical significance. The two-tailed  $P$  value was calculated using the unpaired  $t$  test. The degree of freedom was 18 ( $2n - 2$ ) for all data sets. The alpha level for all tests was chosen as 1% (0.01). When a test of significance gives a  $P$  value lower than 0.01 (alpha level), such results are referred to as statistically significant.

**Microfluidic Device Fabrication.** The microfluidic device was cast in polydimethylsiloxane (PDMS, Sylgard 184, Dow Corning) using standard soft lithography protocols.<sup>45</sup> A 100- $\mu$ m deep master pattern was created on a silicon wafer (Silicon Quest) using SPR-220 resist (Microposit) and deep reactive ion etching (Alcatel). The master was exposed to 1H,1H,2H,2H-perfluorooctyl-trichlorosilane (Sigma Aldrich) to minimize adhesion of PDMS during the peeling step. After the PDMS was peeled off, the inlet and outlet regions were opened by drilling, and the device was sealed to a No. 1 glass coverslip (VWR). Fluid flow through the channel was controlled by syringe pumps (KDS 200 and 220, KD Scientific), connected by polyethylene tubing to the device.

**Fluorescence Imaging (Epifluorescence Imaging).** Chemotaxis of ensembles of enzyme molecules in the presence of a substrate concentration gradient was studied using epifluorescence imaging. This optical setup comprised an Olympus IX71 inverted microscope with a 100 W halogen lamp. Excitation light was passed through the appropriate filter cube (Chroma Technology), depending on the excitation/emission wavelengths of the dye, before it was focused into the sample through a 20 $\times$  objective (LCPlanFl20X/0.40Ph100, Olympus). Fluorescence emission was collected by the objective, passed through interference filters, and detected by a high-sensitivity pco.1600 CCD camera (Cooke Corporation) with a resolution of 1600 pixels  $\times$  1200 pixels and peak quantum efficiency of 55% at 500 nm wavelength.

**Confocal Microscope Imaging.** Confocal images were acquired using a Leica TCS SP5 laser scanning confocal inverted microscope (LSCM, Leica Microsystems) with a 20 $\times$  objective (HCX PL APO

CS, 0.70 NA) incorporated in it. The confocal images were obtained at 514 nm excitation (Ar-ion laser, 65 mW) directed through a double dichroic mirror (DD 458/514), with emission filters set between 560 and 600 nm. The plane of interest (along the  $z$ -axis) for confocal imaging was chosen such that fluorescence intensity was captured from the plane that is half of the height into the channel.

Videos were recorded and analyzed using Image software. In each experiment, the mean fluorescence intensity was calculated from three videos. Each video is a collection of 50–100 images. A region of interest (ROI) was selected along the channel, and the stack-averaged fluorescence intensity was plotted as a function of distance along the width of the channel.

Lateral shifts were calculated by first selecting the central pixel inside the ROI and measuring its fluorescence intensity in the absence of substrate. Then, in the presence of substrate, the ROI was interrogated again to find a pixel with a fluorescence intensity equivalent to that of the one previously measured. The lateral distance of this new pixel from the center of the channel was taken to be the lateral shift. The central pixel was chosen to calculate the lateral shifts in our measurements, as the enzyme molecules will experience maximum gradient in substrate concentration at this point.

**Simulation of Enzyme Chemotaxis Using COMSOL Multiphysics.** To simulate enzyme chemotaxis in the presence of a substrate gradient, we coupled the physics of *Transport of Diluted Species* and *Laminar Flow* of liquids in *COMSOL Multiphysics* (v4.3). These physics are available within the *Chemical Species Transport and Fluid Flow* modules of the software. For stationary state solutions, the equations that govern the convective and diffusive transport of species were  $\nabla \cdot (-D_i \nabla c_i + c_i \mathbf{u}) = 0$ , where  $D_i$  denotes the diffusion coefficient of the species ( $\text{m}^2/\text{s}$ ),  $c_i$  is the species concentration ( $\text{mol}/\text{m}^3$ ), and  $\mathbf{u}$  is the velocity ( $\text{m}/\text{s}$ ). This was supplemented with a flux balance condition for various species,  $N_i = -D_i \nabla c_i + \mathbf{u} c_i$ . The flow of liquid within the microchannel was described by the Navier–Stokes equations given by  $\rho(\mathbf{u} \cdot \nabla) \mathbf{u} = \nabla \cdot [-p\mathbf{I} + \mu(\nabla \mathbf{u} + (\nabla \mathbf{u})^T)] + F$  and  $\rho(\nabla \cdot \mathbf{u}) = 0$ , where  $\rho$  is the density ( $\text{kg}/\text{m}^3$ ),  $\mathbf{u}$  is the velocity ( $\text{m}/\text{s}$ ),  $\mu$  is the viscosity ( $\text{Pa}\cdot\text{s}$ ),  $p$  is the pressure (Pa), and  $F$  is the body force per unit volume ( $\text{N}/\text{m}^3$ ). The modeled fluids are liquids with a viscosity of  $10^{-3}$  Pa·s and density  $10^3$  kg/m<sup>3</sup>. No slip boundary condition was set at the walls of the microchannel. The flux of liquid through the boundary walls and the value of the liquid pressure at the outlet were also set to zero.

In the case of urease, enzyme solutions of concentration  $10^{-3}$  mol/m<sup>3</sup> were allowed to flow in through the lower inlet of the microchannel. In conditions of no substrate, the diffusion coefficient of urease was taken to be  $3.18 \times 10^{-11}$  m<sup>2</sup>/s (zero substrate diffusivity value measured in experiments). Next, the simulation was run for a substrate (urea) flow (initial concentration of  $10^3$  mol/m<sup>3</sup>) through the upper inlet. The diffusion coefficient of urea, in this case was kept fixed at  $1.09 \times 10^{-9}$  m<sup>2</sup>/s, decided by the hydrodynamic radius of urea and the value of solution viscosity. However, the diffusion coefficient of urease was expressed as a function of local substrate (urea) concentration as  $D = 3.18 \times 10^{-11} + 9.03 \times 10^{-12}(\sqrt{c}/(0.65 + \sqrt{c}))$ , where  $c$  is the concentration of urea in mol/m<sup>3</sup> and  $D$  is the enhanced diffusivity of urease in m<sup>2</sup>/s. The functional form of dependence of  $D$  on  $c$  was determined from the experimentally measured increase in diffusivity of urease with the increase in urea concentration (see Figure S7, SI).

Simulations for catalase were carried out in a similar manner with an enzyme solution of strength  $10^{-3}$  mol/m<sup>3</sup>. The zero substrate diffusivity value of catalase was  $6.01 \times 10^{-11}$  m<sup>2</sup>/s. To establish a substrate gradient across the microchannel interface, H<sub>2</sub>O<sub>2</sub> solution of strength  $10^2$  mol/m<sup>3</sup> was allowed to flow in through the upper inlet of the channel, while the lower inlet allowed the flow of catalase molecules in water/buffer—both at a constant flow speed of  $694 \mu\text{m}/\text{s}$ . The diffusion coefficient of H<sub>2</sub>O<sub>2</sub> molecule was taken to be  $1.0 \times 10^{-9}$  m<sup>2</sup>/s, whereas that of catalase was expressed as function of local H<sub>2</sub>O<sub>2</sub> concentration as  $D = 6.01 \times 10^{-11} + 2.80 \times 10^{-11}(c/(6.3+c))$ , where  $c$  is the concentration of H<sub>2</sub>O<sub>2</sub> in mol/m<sup>3</sup> and  $D$  is the enhanced diffusivity of catalase in m<sup>2</sup>/s. The functional form of dependence of  $D$  on  $c$  was determined from the experimentally measured increase in

diffusivity of catalase with the increase in H<sub>2</sub>O<sub>2</sub> concentration (see Figure S8, SI).

**Diffusion Measurements of Inhibited Catalase (Fluorescently Labeled) in the Presence of Active Catalase (Unlabeled) and Hydrogen Peroxide.** Bovine liver catalase (Sigma-Aldrich; see Figure S9B, SI) was labeled with an amine-reactive rhodamine dye (ex/em: 552/575; Thermo Fisher Scientific). Labeling of catalase ( $4 \mu\text{M}$ ) with the fluorescent dye ( $40 \mu\text{M}$ ) was performed in a gently stirred, room temperature 100 mM phosphate buffer (pH 7.2) for 2–3 h (see Figure S9D, SI). The enzyme–dye complex was further purified using membrane dialysis (10 kDa pores; Amicon ultra-4 centrifugal filter unit, Millipore) to reduce free-dye concentration. Fluorescently labeled catalase ( $4 \mu\text{M}$ ) was incubated with 0.5 M NaCN (inhibitor) in deionized water overnight. Membrane dialysis (10 kDa pores; Amicon ultra-4 centrifugal filter unit, Millipore) was used to separate the enzyme–dye complex from unreacted inhibitor.

Different concentrations of hydrogen peroxide solution (0, 0.001, 0.01, and 0.1 M) in deionized water were prepared. Fluorescently labeled inactive catalase (5 nM) and active catalase (5 nM, unlabeled) were added, and diffusion measurements of inhibited catalase were carried out immediately, using FCS in a fashion similar to that described earlier.

**Decomposition of Hydrogen Peroxide in the Presence of Active and Inhibited Catalase Samples.** The decomposition of hydrogen peroxide, monitored using a UV–vis spectrophotometer,<sup>46</sup> was assessed in the presence of active catalase, inactive catalase, and a mixture of active and inactive catalase. The enzyme samples were mixed with H<sub>2</sub>O<sub>2</sub> solution (0.035% w/w) in deionized water in a quartz cuvette, and the decrease in absorbance of H<sub>2</sub>O<sub>2</sub> at 240 nm was observed over time. In between absorbance readings, the cuvette was stirred to dislodge O<sub>2</sub> bubbles formed on the sides of the cuvette.

**Viscosity Measurements.** The viscosities of different hydrogen peroxide (substrate) solutions were measured using a cone–plate viscometer (Haake Rotovisco 1, Thermo Electron).

**Behavior of Free Dye Molecules Toward Substrate Concentration Gradient.** Fluorescence imaging was used to characterize the movement of free dye along a substrate concentration gradient. A ‘Y’-shaped microfluidic channel with two inlets, one for dye and the other for buffer or substrate, was used to generate the substrate gradient (Figure 2). Lateral spreading of the dye at a defined location in the microchannel was measured. The directional behavior of NHS-Rhodamine (used to label catalase) was studied in the presence of water, 10 mM hydrogen peroxide, and 100 mM glucose. Fluorescence intensity profiles were plotted as a function of lateral position along the width of the channel in order to measure the lateral spreading of the dye molecules. In a separate control, identical experiments were performed with free Dylight 549 dye molecules (used to label urease) in the presence of 150 mM PBS and 1 M urea (in 150 mM PBS).

**Behavior of Quantum Dots Toward Substrate Concentration Gradient.** Fluorescence imaging was used to characterize the movement of quantum dots (QDots), 20 nm in diameter, along a substrate concentration gradient. A ‘Y’-shaped microfluidic channel with two inlets, one for Qdots and active catalase (unlabeled), and the other for water or substrate, was used to generate the substrate concentration gradient (Figure 2). Lateral spreading of the QDots at a defined location in the microchannel was measured in the presence of water and 10 mM hydrogen peroxide. Similar experiments were performed with QDots and urease to observe the shift in fluorescence intensity toward 1 M urea as compared to buffer.

## ■ ASSOCIATED CONTENT

### 📄 Supporting Information

Details of DLS measurements, enzyme activity assessment, bulk temperature estimation, fitting of enhanced enzyme diffusivities, and description of supplementary experimental methods and results. This material is available free of charge via the Internet at <http://pubs.acs.org>.

## ■ AUTHOR INFORMATION

## Corresponding Author

asen@psu.edu; pjbio@engr.psu.edu

## Author Contributions

<sup>§</sup>K.K.D., H.S.M., and T.T. contributed equally to this work.

## Notes

The authors declare no competing financial interest.

## ■ ACKNOWLEDGMENTS

We gratefully acknowledge the Penn State MRSEC under NSF Grant DMR-0820404 for supporting this work. We acknowledge the Research Computing and Cyberinfrastructure unit of Information Technology Services at The Pennsylvania State University for providing advanced computing resources and services that have contributed to the research results reported in this paper (<http://rcc.its.psu.edu>). We thank Prof. Darrell Velegol for fruitful discussions. We also thank Dr. Ran Liu for his help in preparing manuscript figures.

## ■ REFERENCES

- (1) Goel, A.; Vogel, V. *Nat. Nanotechnol.* **2008**, *3*, 465–475.
- (2) Lipowsky, R.; Beeg, J.; Dimova, R.; Klumpp, S.; Liepelt, S.; Müller, M. J. I.; Valleriani, A. *Biophys. Rev. Lett.* **2009**, *4*, 77–137.
- (3) Puchner, E. M.; Gaub, H. E. *Annu. Rev. Biophys.* **2012**, *41*, 497–518.
- (4) Adler, J. *Science* **1969**, *166*, 1588–1597.
- (5) Berg, H. C.; Brown, D. A. *Nature* **1972**, *239*, 500–504.
- (6) Wang, J. *ACS Nano* **2009**, *3*, 4–9.
- (7) Sanchez, S.; Pumera, M. *Chem.—Asian J.* **2009**, *4*, 1402–1410.
- (8) Paxton, W. F.; Sundararajan, S.; Mallouk, T. E.; Sen, A. *Angew. Chem., Int. Ed.* **2006**, *45*, 5420–5429.
- (9) Hong, Y.; Velegol, D.; Chaturvedi, N.; Sen, A. *Phys. Chem. Chem. Phys.* **2010**, *12*, 1423–1425.
- (10) Ozin, G. A.; Manners, I.; Fournier-Bidoz, S.; Arsenault, A. *Adv. Mater.* **2005**, *17*, 3011–3018.
- (11) Paxton, W. F.; Sen, A.; Mallouk, T. E. *Chem.—Eur. J.* **2005**, *11*, 6462–6470.
- (12) Sengupta, S.; Ibele, M. E.; Sen, A. *Angew. Chem., Int. Ed.* **2012**, *51*, 8434–8445.
- (13) Mei, Y.; Solovev, A. A.; Sanchez, S.; Schmidt, O. G. *Chem. Soc. Rev.* **2011**, *40*, 2109–2119.
- (14) Wang, J.; Manesh, K. M. *Small* **2010**, *6*, 338–345.
- (15) Mirkovic, T.; Zacharia, N. S.; Scholes, G. D.; Ozin, G. A. *Small* **2010**, *6*, 159–167.
- (16) Muddana, H. S.; Sengupta, S.; Mallouk, T. E.; Sen, A.; Butler, P. J. *J. Am. Chem. Soc.* **2010**, *132*, 2110–2111.
- (17) Srere, P. A. *Ann. Rev. Biochem.* **1987**, *56*, 89–124.
- (18) Gullapalli, R. R.; Tabouillot, T.; Mathura, R.; Dangaria, J. H.; Butler, P. J. *J. Biomed. Opt.* **2007**, *12*, 014012 (1–17).
- (19) Lakowicz, J. R. *Principles of Fluorescence Spectroscopy*, 3rd ed.; Springer: New York, 2006.
- (20) Chance, B. *J. Biol. Chem.* **1949**, *179*, 1299–1309.
- (21) Yin, H.; Wang, M. D.; Svoboda, K.; Landick, R.; Block, S. M.; Gelles, J. *Science* **1995**, *270*, 1653–1657.
- (22) Mehta, A. D.; Rief, M.; Spudich, J. A.; Smith, D. A.; Simmons, R. M. *Science* **1999**, *283*, 1689–1695.
- (23) Mahadevan, L.; Matsudaira, P. *Science* **2000**, *288*, 95–99.
- (24) Hong, Y.; Blackman, N. M. K.; Kopp, N. D.; Sen, A.; Velegol, D. *Phys. Rev. Lett.* **2007**, *99*, 178103 (1–4).
- (25) Yu, H.; Jo, K.; Kounovsky, K. L.; de Pablo, J. J.; Schwartz, D. C. *J. Am. Chem. Soc.* **2009**, *131*, 5722–5723.
- (26) Sanchez, S.; Solovev, A. A.; Mei, Y.; Schmidt, O. G. *J. Am. Chem. Soc.* **2010**, *132*, 13144–13145.
- (27) Manesh, K. M.; Cardona, M.; Yuan, R.; Clark, M.; Kagan, D.; Balasubramanian, S.; Wang, J. *ACS Nano* **2010**, *4*, 1799–1804.
- (28) Najafi, A.; Golestanian, R. *Europhys. Lett.* **2010**, *90*, 68003 (1–6).
- (29) Miño, G.; Mallouk, T. E.; Darnige, T.; Hoyos, M.; Dauchet, J.; Dunstan, J.; Soto, R.; Wang, Y.; Rousselet, A.; Clement, E. *Phys. Rev. Lett.* **2011**, *106*, 048102 (1–4).
- (30) Kurtuldu, H.; Guasto, J. S.; Johnson, K. A.; Gollub, J. P. *Proc. Natl. Acad. Sci. U.S.A.* **2011**, *108*, 10391 (1–5).
- (31) Jiang, H.-R.; Yoshinaga, N.; Sano, M. *Phys. Rev. Lett.* **2010**, *105*, 268302 (1–4).
- (32) Golestanian, R.; Liverpool, T. B.; Ajdari, A. *Phys. Rev. Lett.* **2005**, *94*, 220801 (1–4).
- (33) Howse, J. R.; Jones, R. A. L.; Ryan, A. J.; Gough, T.; Vafabakhsh, R.; Golestanian, R. *Phys. Rev. Lett.* **2007**, *99*, 048102 (1–4).
- (34) Córdova-Figueroa, U. M.; Brady, J. F. *Phys. Rev. Lett.* **2008**, *100*, 158303 (1–4).
- (35) Ke, H.; Ye, S.; Carroll, R. L.; Showalter, K. J. *Phys. Chem. A* **2010**, *114*, 5462–5467.
- (36) Sakaue, T.; Kapral, R.; Mikhailov, A. S. *Eur. Phys. J. B* **2010**, *75*, 381–387.
- (37) Cressman, A.; Togashi, Y.; Mikhailov, A. S.; Kapral, R. *Phys. Rev. E* **2008**, *77*, 050901 (1–4).
- (38) Golestanian, R. *Phys. Rev. Lett.* **2010**, *105*, 018103 (1–4).
- (39) Astumian, R. D. *Annu. Rev. Biophys.* **2011**, *40*, 289–313.
- (40) Astumian, R. D. *Science* **1997**, *276*, 917–922.
- (41) Reimann, P. *Phys. Rep.* **2002**, *361*, 57–265.
- (42) Elson, E. L.; Magde, D. *Biopolymers* **1974**, *13*, 1–27.
- (43) Magde, D.; Elson, E. L.; Webb, W. W. *Biopolymers* **1974**, *13*, 29–61.
- (44) Krichevsky, O.; Bonnet, G. *Rep. Prog. Phys.* **2002**, *65*, 251–297.
- (45) Xia, Y.; Whitesides, G. M. *Annu. Rev. Mater. Sci.* **1998**, *28*, 153–184.
- (46) Beers, R. F., Jr.; Sizer, I. W. *J. Biol. Chem.* **1952**, *195*, 133–140.